NANO LETTERS

2007
Vol. 7, No. 12
3628−3632

Moiré Patterns in Superimposed Nanoporous Thin Films Derived from Block-Copolymer Assemblies

Valeriy Luchnikov,*,† Alexey Kondyurin,‡ Petr Formanek,§ Hannes Lichte,§ and Manfred Stamm†

Leibniz Institute of Polymer Research Dresden, D-01069 Dresden, Germany, University of Sydney, School of Physics, A28, The University of Sydney, NSW 2006, Australia, and Technical University of Dresden, Triebenberg Lab, D 01062 Dresden, Germany

Received July 28, 2007; Revised Manuscript Received October 21, 2007

ABSTRACT

Nanoscale rotation moiré patterns are observed in double-layer nanoporous thin films produced with use of block-copolymer self-assembly. Periodic hexagonal moiré superstructures appear when the films possessing long-range order are superimposed at small misorientation angles. Overlapping films misoriented by angles close to 30° generate aperiodic quasi-crystal-like superstructures with 5-fold symmetries. The stacking of the disordered nanoporous films produces labyrinth-like patterns. Block-copolymer moiré superstructures are promising as nanolithography masks with controllable morphology and periodicity.

Moiré patterns are common in everyday life and often occur when two lattices overlap one another (e.g., in folds of sheer curtains). They were used in technique[1] and even inspired artists.[2] Before the invention of holographic interferometry, moiré patterns constituted a popular tool to study deformations, which can be calculated from the moiré fringes formed by two interfering line screens, one is printed on the loaded solid model and the other is used as the reference.[1] The moiré phenomenon is omnipresent also at the nanoscale. Rotation moiré superlattices were observed in graphite layers since early days of scanning tunneling microscopy (STM). The origin of these superlattices is actively debated because of importance of pyrolytic graphite as a standard substrate for STM measurements. It is believed that moiré fringes in this system can appear due to interference of tunneling currents to multiple tips of the STM probe scanning adjacent crystalline grains, which are rotated with respect to each other.[3] Hexagonal moiré superstructures can arise also in folded-back graphite monolayers as the result of the interaction of the top and the bottom layers.[4] Regular hexagonal arrays of morphological units, identified as rotation moiré patterns, were observed by transmission electron microscopy (TEM) of stained folded biological membranes.[5] These patterns prove indirectly the high degree of crystalline order of the cell's membranes formed by lipid molecules. Recently, moiré fringes were shown to be a powerful tool for the generation of micro-and nanoscale patterns and two-dimensional (2D) superlattices. Regular arrays of dislocation lines were obtained by twisting two identical silicon wafers one against the other at a precisely controlled angle and bonding them together to make a bicrystal.[6] Selective etching of the screw dislocations generated in this way permits controlled fabrication of nanodot arrays with 2−100 nm spacing. Moiré fringes characterized by a few micrometer spacing were synthesized by the two-step nanoindentation lithography on aluminum substrates with a master stamp consisting of regular arrays of Si_3N_4 micropyramids.[7] The fringes obtained after amplification of the indentations by anodization realize novel kinds of micropatterns, which are hard to achieve with current state-of-the-art conventional lithography.

In this paper, we report the first observation of rotation moiré patterns produced by overlapping block-copolymer (BCP) thin films self-assembled in the well-defined hexagonal morphology. Self-assembled block-copolymer films have attracted much interest of material scientists in the last years as nanolithography masks and templates for synthesis of nanoparticles[8] and membranes for ultra-filtration.[9] We obtain nanoporous BCPs by the approach first suggested by Ikkala et al.[10] and developed also by our research group.[11] The films are prepared by codissolving polystyrene-block-poly(4-vinyl pyridine) (PS-b-P4VP) and 2-(4′-hydroxybenzeneazo) ben-

* Corresponding author. E-mail: luchnikov@ipfdd.de; luchnikov@yahoo.com Tel: +49(0)351-4658272. Fax: +49(0)351-4658281.
† Leibniz Institute of Polymer Research Dresden.
‡ The University of Sydney.
§ Technical University of Dresden.

10.1021/nl071844k CCC: $37.00
Published on Web 11/02/2007

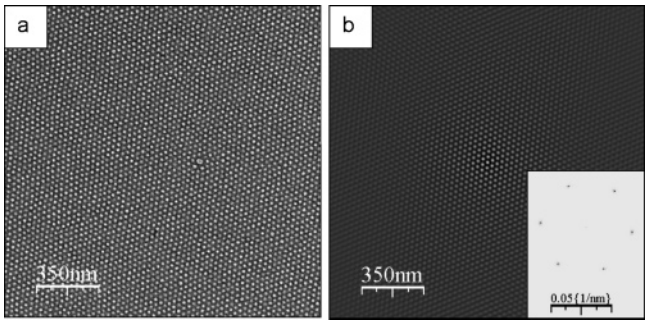

Figure 1. The central part of a hexagonal morphology monodomain of a single-layer film. (a) TEM micrograph. The view size is 1.8 μm. The absence of the grain boundaries is evident if one observes the figure at a small angle to the page. (b) Autocorrelated image of (a). Inset: power spectrum density (only the peaks of the basic frequency are shown).

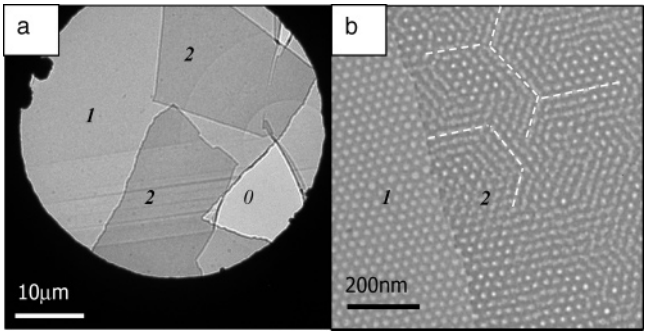

Figure 2. (a) TEM image of a nanostructured thin film floated and picked-up on a copper grid. (b) The boundary of one of the single- and the double-layer zones, shown on the (a) with zoom-in micrograph. A few moiré fringes are designated with a dashed white line for eye-guiding. On the both images, the numbers indicate the number of the layers in the corresponding zones.

zoic acid (HABA) that is associated with the P4VP block by hydrogen bonds. P4VP + HABA complexes constitute the minority component of the system and form cylinders, which are aligned along the normal direction to the film and embedded into the PS matrix. Hexagonal ordering of the BCP morphology was greatly enhanced by vapor annealing.[12] The nanoporous films were obtained by rinsing the low-molecular weight HABA from the cylinder domains. The films were stabilized by plasma immersion implantation, which causes crosslinking and partial or complete carbonization of the polymer.[13] Then the films were floated on the surface of 1 wt % aqueous solution of hydrofluoric acid, picked on metallic microgrids, and investigated by TEM.

The single-layer films are characterized by a high degree of spatial coordination of the pores organized in a triangular lattice with the lattice constant $d \approx 30-35$nm. In our experiments, the monodomains of the triangular morphology are typically $1-3$ μm wide (see Figure 1a and Supporting Information, Figure S1). Long-range order is best proven by the autocorrelated image (Figure 1b) that is calculated as $G(u,v) = \langle I(x+u, y+v)I(x,y)\rangle$, where $I(x,y)$ is the brightness of the image at the point (x,y), and brackets denote averaging over all points. By the Wiener−Khinchin theorem, the autocorrelation function is related via Fourier transform to the power spectrum density (PSD) of the image, $S(k_x,k_y)$. The latter is shown as the inset in Figure 1b. In the explored films, only part of the pores were really empty, whereas the rest of them were partially filled by the carbonized material. Nevertheless, all the pores are clearly identified due to their better transparency to the electron beam.

The overlapping layers (Figure 2) appeared in our experiments occasionally during the floating and picking-up procedures. Apparently, small fragments of the film were deposited over the bigger film parts during drying of the solution on the top of the grids. The multilayered films arise also by occasional back-folding of the nanoporous films; in that case more than two superimposed layers may appear (see Supporting Information, Figure 2). For the sake of clarity, we consider here only the films consisting of two layers. At low magnification (Figure 2a), the double layer films differ from the single layer ones only by the transparency to the electron beam. A high-resolution micrograph (Figure 2b) shows that superposition of the top and the bottom hexagonally ordered layers gives rise to morphological features, which can be recognized as rotation moiré patterns.

TEM micrographs of several double-layer highly ordered films, overlapped at different angles, and arising moiré patterns are shown on Figure 3. The brightness of the image (the mass-thickness contrast) is proportional to the transparency of the film to the electron beam, defined as $T(x,y) = J(x,y)/J_0 = \exp\{-h(x,y)/\lambda\}$, where $J(x,y)$ and J_0 are the intensities of the beam after and before the film, respectively, λ is the mean free-path length of electrons, and $h(x,y)$ is the thickness of the film.[14] Therefore, the transparency of the double layer film is the product of the transparencies of the single layers, $T(x,y) = \exp\{-(h_1 + h_2)/\lambda\} = T_1(x,y)T_2(x,y)$. According to the elementary theory,[15,16] the periodicity D of rotation moiré fringes depends on the lattice constant of a single layer, d, and the misorientation angle α by the Rayleigh relation, $D = d/[2\sin(\alpha/2)]$. Note that superimposed triangular pore lattices born a hexagonal moiré superstructure. The average feature size of the hexagonal pattern shown on Figure $3a_1$ is $D \approx 150$ nm, as estimated by measuring the period of the pattern on the autocorrelated image (Figure $3a_2$). The angle α for a pair of the overlapped films can be found by measuring the angular splitting of the PSD peaks (inset in the Figure $3a_2$). The experimentally observed parameters $D = 150$ nm, $d \approx 33$nm, and $\alpha = 13°$ are in good correspondence with each other, predicted by the theory. Besides the main peaks, related to triangular pore lattices of the top and the bottom layers, PSD of the double layer film contains a hexagonal set of low-frequency peaks (marked by the dashed line circle on the inset in the Figure $3a_2$), which can be attributed to the periodic moiré pattern. These peaks can be described as a result of convolution of Fourier transforms, calculated for single layer films, disoriented by the angle α (see ref 14 and Supporting Information, Figure S3). Inverse Fourier transform of the reciprocal lattice of the double layer film with use of the low-pass filter (indicated by the dashed line in the inset to Figure $3a_2$) reveals a hexagonal superstructure with the periodicity of the moiré fringes (Figure $3a_3$). Our interpretation of the moiré

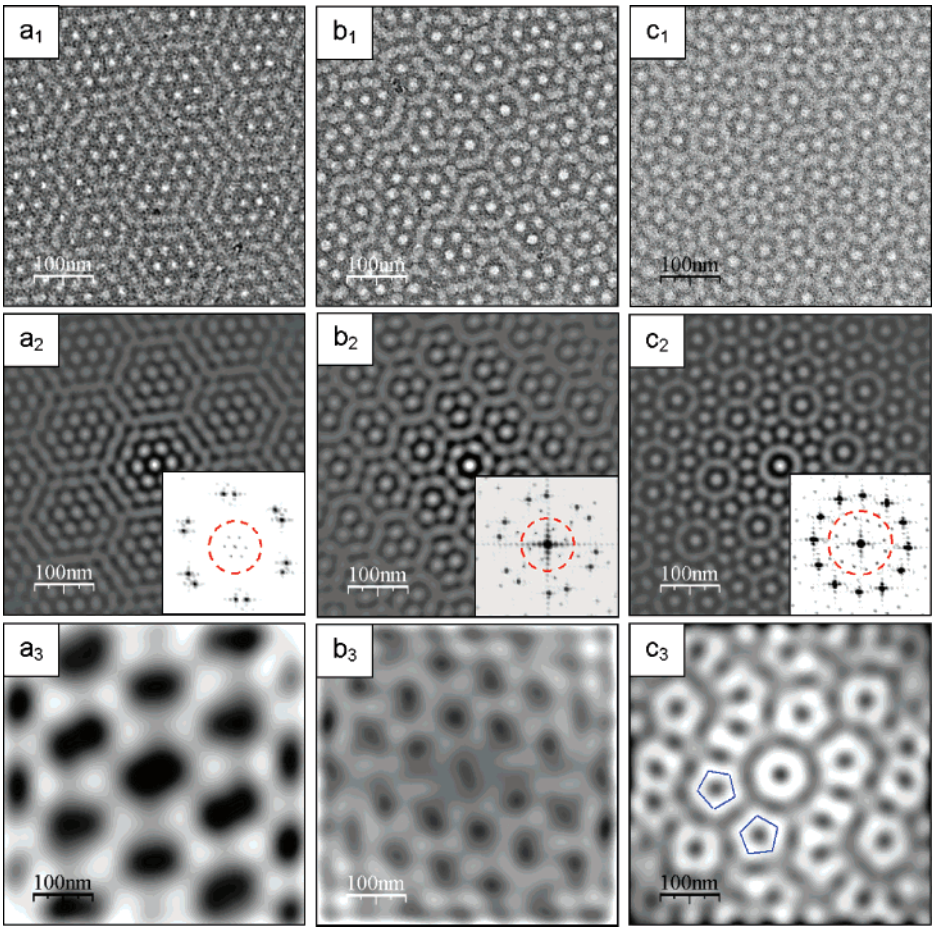

Figure 3. Upper row: TEM images of double-layer nanoporous films for different misorientation angle, α, (a_1), $\alpha_1 = 13°$; (b_1), $\alpha_2 = 19°$, (c_1), $\alpha_2 = 29°$. Middle row: (a_2), (b_2), and (c_2) are the autocorrelated images of (a_1), (b_1), and (c_1), respectively. The insets show the Fourier transforms of the autocorrelated images. The dashed line circles enclose the low-frequency impulses corresponding to the moiré superstructures. Bottom row: The superstructures visualized by low-pass filtering of the autocorrelated images. The pentagonal rings on (c_3) are drawn for eye guiding. The analysis of the patterns was performed with the use of *WSxM* and *ImageJ* freeware.

phenomenon in the overlapped nanoporous films is supported by a computer experiment (see Supporting Information, Figure S4.).

It is clear that moiré effect can be observed only if the size of grains, superposed at a misorientation angle α, is not smaller than the periodicity of moiré fringes predicted by the Rayleigh relation for this angle. For example, for $\alpha = 5°$ the grain's width should be not less than approximately 11 interpore distances. For our films, this corresponds to the minimal grain size $D_{gr} \approx 350$ nm. On the other hand, for a given size D_{gr} of the grains, the minimal misorientation angle for which the moiré effect can be detected is estimated as $\alpha_{min} = 2 \arcsin(d/2D_{gr})$. For 3 μm wide grains, which are typical for our films, the misalignment angle can be as small as $\approx 0.3^0$.

A moiré pattern generated by two films misoriented at somewhat larger angle, $\alpha = 19°$ is shown on Figure $3b_1$. The hexagonal motifs on this image are smaller and less evident than the similar motifs on the previously discussed pattern shown on Figure 3a. Yet, the moiré fringes are clear on the autocorrelated image (Figure $3b_2$). The superlattice obtained by low-pass filtering of the pattern (Figure $3b_3$) has the lattice constant $D \approx 84$ nm, which is in good correspondence with the theoretical value. A new kind of the pattern arises when the misorientation angle approaches the maximal value (30°, for the triangular lattice). Figure $3c_1$ shows the fringes that appear in the films overlapped at $\alpha = 29°$. The pattern is aperiodic, yet strongly autocorrelated, as Figure $3c_2$ clearly indicates. PSD spectrum of the pattern has almost perfect 12-fold symmetry, which is incommensurable with a translational periodicity. Intriguingly, the low-pass filtering of the image reveals quasi-crystal-like fringes possessing 5-fold symmetry (Figure $3c_3$ and Supporting Information, Figure S5).

In a few experiments, we observed the films in which the pore arrangement does not possess long range order. This is the case of poorly annealed BCP morphologies, in which only a small fraction of the pores is hexagonally coordinated. Superimposing of such films produces disordered labyrinth-like patterns (Figure 4). A similar result is produced by overlapping polycrystalline films with small average sized 2D crystal grains (the limitations on the size of the grains are discussed above). The distribution of color intensity of the TEM micrographs (see the histograms on Figure 4) correlates with the thicknesses of the film. The distribution is trimodal for the double-layer film, unlike bimodal distributions for the single-layer ones. The three modes of the color intensity correspond to "matrix-against-matrix", "matrix-

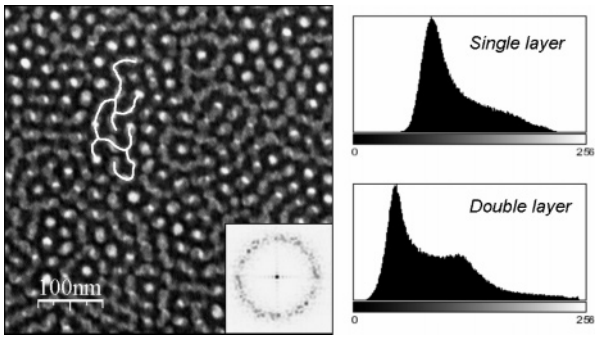

Figure 4. TEM image of a film produced by the superimposing of two layers with a poor degree of pore coordination. Inset: PSD of the image. One of the clusters of the matrix-against-pore overlapping is marked by the white line. The histograms show the distributions of the color shades of a single layer film (such as presented on Figure 1a) and the double layer film. The brightness correlates with the film transparency for the electron beam. See also Supporting Information, Figure S6.

against-pore" and "pore-against-pore" overlapping situations, whereas in the single-layer films only the color shades corresponding to the matrix and the pores are present. It is the matrix-against-pore regions that form extended clusters of intermediate degree of transparency for the electron beam. Note that no similar clusters are seen on TEM-images of single layer films.

Discussion and Outlook. We have reported the first observation of rotation moiré patterns in superimposed nanoporous films derived from block-copolymer assemblies. Periods of moiré superstructures, arising in overlapped BCP nanoporous films, spun from dozens to hundreds of nanometers. Thus, the BCP-generated rotation moiré fringes cover the length scale interval between the moiré superstructures produced by twisting and merging of crystals[6] and the moiré patterns made by microfabrication tools.[7] At small misorientation angles, periodicity of hexagonal moiré fringes is well described by the Rayleigh relation. Large misorientation angles result in complex aperiodic fringes, which resemble 2D quasi-crystalline tilings.[17] Misorientation angle between the pore lattices of the top and the bottom layers can be determined as the angular splitting of the PSD peaks of the patterns. Superposition of disordered nanoporous films results in labyrinth-like morphologies, which are not present in single-layer films.

Moiré patterns observed in overlapped nanostructured thin films can provide new rich opportunities for nanofabrication. Recently, BCP films were shown to have great potential as masks for nanolithography.[8,18] Morphology of nanoporous templates was transferred into substrates by reactive ion etching,[18] vacuum metal evaporation,[19] and electrodeposition.[20] Yet the variety of structures, which can be produced with the use of single-layer BCP templates, is constrained to self-assembled morphologies, such as hexagonally coordinated cylindrical domains or lamellae. The variety of highly correlated patterns can be greatly broadened by using the moiré effect for the nanoporous films. Some of theoretically possible masks are shown in Supporting Information, Figure 7. Although the patterns that we discussed in our work were obtained by random deposition of the films over each other, we believe that a technique of the reproducible nanomask fabrication can be developed. The major prerequisite for such a technique is the control of the nanopore morphology over large areas. This requirement was recently fulfilled by using the top-down control of the block-copolymer self-assembly on micropatterned substrates. It was demonstrated that the most dense planes of the 2D triangular BCP morphology align themselves along the edges of topographic or chemical patterns, created by means of e-beam lithography or microcontact printing.[21] In this way, a necessary orientation of a BCP lattice can be induced over the entire substrate surface. The oriented films can be then merged together at a desired angle (see Supporting Information, Figure 8). As noted in ref 7, the rotation angle is the same for all the length scales of a system, consisting of two mutually rotating parts. Therefore, the relative orientation of the nanostructures can be controlled with high accuracy by varying the angle between the substrates. To release the moiré pattern after the film's merging, one of the substrates can be made cleavable. NaCl crystals seem to be well suited for this purpose, because they are water solvable and have been already used as substrates for well-ordered block-copolymer assemblies.[22] On the other hand, patterning of NaCl crystals by means of e-beam lithography was also demonstrated.[23] In a different approach, a macroscopic orientation of BCP lamellar morphologies was induced by "micromolding" technique with the use of a micropatterned elastomeric stamp.[24] Another principle possibility of formation of the moiré-like superlattices is a consecutive exposure of an electron beam resist through a single-layered nanoporous film, at two different mutual angles of the film and the substrate (see Supporting Information, Figure 9). Controlled formation of the moiré nanomasks and superlattices with the use of BCP films will be addressed in our future studies.

Acknowledgment. This research was supported by the European Network of Excellence Nanofun-Poly and the Deutsche Forschungsgemeinschaft (Project STA 31-1 within priority program SPP1165/2). A.K. thanks Leibniz Institute of Polymer Research Dresden for hospitality and Humboldt foundation for the financial support. P.F. acknowledges financial support by the European Union (Framework 6 Integrated Infrastructure, Reference 026019 ESTEEM).

Supporting Information Available: Figure S1: TEM micrograph of a 3.1 μm-wide monodomain of triangular lattice of pores. Figure S2: TEM micrographs of folded-back nanoporous films. Figure S3: analysis of a moiré pattern in the reciprocal space. Figures S4−S6: computer simulation of the moiré phenomenon in porous films. Figures S7−S9: illustrations to proposed future research. This material is available free of charge via the Internet at http://pubs.acs.org.

References

(1) Sciammarella, C. A.; Durelli, A. J. *Am. Soc. Civ. Eng.* **1962**, *127*, 582−603.
(2) The effect was used, for example, in the artworks of Victor Vasarely and Werner Witschi. See also: Oster, G. *Adv. Biol. Med. Phys*. **1977**, *16*, 333−347.

(3) Albrecht, T. R.; Mizes, H. A.; Mizes, J.; Nogami, J.; Park, S.; Quate, C. F. *Appl. Phys. Lett.* **1988**, *52*, 362−364.
(4) Beyer, H.; Müller, M.; Schimmel, Th. *Appl. Phys. A* **1999**, *68*, 163−166.
(5) Glaubert, A. M. *J. Cell. Sci., I* **1966**, 425−428.
(6) Sass, S.; Hines, M. *Appl. Phys. Lett.* **2001**, 78, 2205−2207.
(7) Choi, J.; Wehrspohn, R. B.; Gösele, U. *Adv. Mater.* **2003**, *15*, 1531−1534.
(8) Hamley, I. W. *Nanotechnology* **2003**, *14*, R39−R54.
(9) Yang, S. Y.; Ryu, I.; Kim, H. Y.; Kim, J. K.; Jang, S. K.; Russell, T. R. *Adv. Mater*. **2006**, *18*, 709−712.
(10) Ruokolainen, J.; Mäkinen, R.; Torkkeli, M.; Mäkelä, T.; Serimaa, R.; ten Birke, G.; Ikkala, O. *Science* **1998**, *280*, 557−560.
(11) Sidorenko, A.; Tokarev, I.; Minko, S.; Stamm, M. *J. Am. Chem. Soc.* **2003**, *125*, 12211−12216.
(12) Fukunaga, K.; Elbs, H.; Magerle, R.; Krausch, G. *Macromolecules* **2000**, *33*, 947−953.
(13) (a) Gan, B. K.; Bilek, M. M. M.; Kondyurin, A.; Mizuno, K.; McKenzie, D. R. *Nucl. Instr. Methods Phys. Res. B* **2006**, *247*, 254−260. (b) Kondyurin, A.; Bilek, M. M. M.; Janke, A.; Stamm, M.; Luchnikov, V. *Plasma Process. Polym.* **2007**, *4*, DOI: 10.1002/ppap.200700111, published online.
(14) Reimer, L. *Transmission electron microscopy*; Springer-Verlag: Berlin Heidelberg, 1997; Vol. 36, p 145.
(15) (a) Rayleigh, Lord. *Philos. Mag.* **1874**, *47*, 81−93. (b) Green, T. A.; Weigle, J. *Helv. Phys. Acta* **1948**, *21*, 217−220. (c) Amidror, I. *The theory of the moiré phenomenon*; Kluwer Academic Publisher: Norwell, MA, 2000.
(16) A good brief introduction in the quantitative analysis of the moire phenomenon can be found in Amidror. I.; *J. Opt. Soc. Am. A* **2003**, *20*, 1900−1919.
(17) This resemblance may have deep reasons, because both the moiré fringes and the aperiodic quasi-crystalline tilings are discrete in the reciprocal space. Discreteness of the diffraction patterns in the absence of spatial periodicity is an intrinsic property of quasi-crystals, fixed in a modern definition of a crystal by the International Union of Crystallography, *Acta Cryst.* **1992**, *A48*, 922−946. (see also http://www.iucr.org/iucr-top/iucr/cac.html).
(18) Park, M.; Harrison, C.; Chaikin, P. M.; Register, R. A.; Adamson, D. H. *Science*, **1997**, *276*, 1401−1404.
(19) Shin, K.; Leach, K. A.; Goldbach, J. T.; Kim, D. H.; Jho, J. Y.; Tuominen, M. T.; Hawker, C. J.; Russell, T. P. *Nano Lett.* **2002**, *2*, 933−936.
(20) Thurn-Albrecht, T.; Schotter, J.; Kästle, G. A.; Emley, N.; Shibauchi, T.; Krusin-Elbaum, L.; Guarini, K.; Black, C. T.; Tuominen, M. T.; Russell, T. P. *Science* **2000**, *290*, 2126−2129.
(21) Cheng, J. Y.; Ross, C. A.; Smith, H. I.; Thomas, E. L. *Adv. Mater*. **2006**, *18*, 2505−2521.
(22) Ludwigs, S.; Böker, A.; Voronov, A.; Rehse, N.; Magerle, R.; Krausch, G. *Nat. Mater.* **2003**, *2*, 744−747.
(23) Stefani, D.; Kratschmer, E.; Beneking, H. *J. Vac. Technol.* **1983**, *1*, 1011−1013.
(24) Li, L.; Yokogama, H. *Adv. Mater.* **2005**, *17*, 1432−1436.

NL071844K